APL Materials

Toward AlGaN channel HEMTs on AlN: Polarization-induced 2DEGs in AlN/AlGaN/AlN heterostructures

Cite as: APL Mater. **10**, 111120 (2022); https://doi.org/10.1063/5.0121195
Submitted: 16 August 2022 • Accepted: 25 October 2022 • Published Online: 23 November 2022

Jashan Singhal, Reet Chaudhuri, Austin Hickman, et al.

openaccess
View Online
Export Citation
CrossMark

ARTICLES YOU MAY BE INTERESTED IN

Record >10 MV/cm mesa breakdown fields in $Al_{0.85}Ga_{0.15}N/Al_{0.6}Ga_{0.4}N$ high electron mobility transistors on native AlN substrates
Applied Physics Letters **120**, 172106 (2022); https://doi.org/10.1063/5.0083966

Realization of homojunction PN AlN diodes
Journal of Applied Physics **131**, 175701 (2022); https://doi.org/10.1063/5.0086314

High electron mobility in AlN:Si by point and extended defect management
Journal of Applied Physics **132**, 185703 (2022); https://doi.org/10.1063/5.0124589

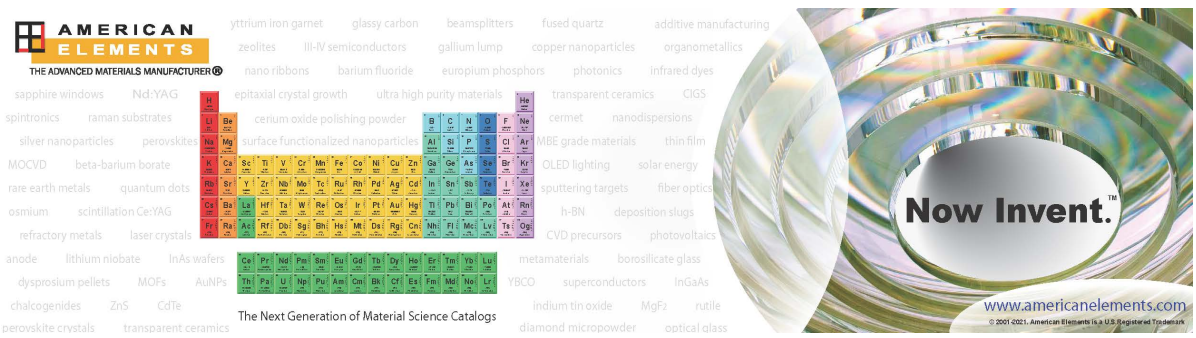

© 2022 Author(s).

AIP Publishing

Toward AlGaN channel HEMTs on AlN: Polarization-induced 2DEGs in AlN/AlGaN/AlN heterostructures

Cite as: APL Mater. 10, 111120 (2022); doi: 10.1063/5.0121195
Submitted: 16 August 2022 • Accepted: 25 October 2022 •
Published Online: 23 November 2022

View Online Export Citation CrossMark

Jashan Singhal,[1,a)] Reet Chaudhuri,[1] Austin Hickman,[1] Vladimir Protasenko,[1] Huili Grace Xing,[1,2,3] and Debdeep Jena[1,2,3]

AFFILIATIONS

[1] School of Electrical and Computer Engineering, Cornell University, Ithaca, New York 14853, USA
[2] Department of Materials Science and Engineering, Cornell University, Ithaca, New York 14853, USA
[3] Kavli Institute at Cornell for Nanoscale Science, Cornell University, Ithaca, New York 14853, USA

[a)] **Author to whom correspondence should be addressed:** js3452@cornell.edu

ABSTRACT

Due to its high breakdown electric field, the ultra-wide bandgap semiconductor AlGaN has garnered much attention recently as a promising channel material for next-generation high electron mobility transistors (HEMTs). A comprehensive experimental study of the effects of Al composition x on the transport and structural properties is lacking. We report the charge control and transport properties of polarization-induced 2D electron gases (2DEGs) in strained AlGaN quantum well channels in molecular-beam-epitaxy-grown AlN/$Al_xGa_{1-x}N$/AlN double heterostructures by systematically varying the Al content from $x = 0$ (GaN) to $x = 0.74$, spanning energy bandgaps of the conducting HEMT channels from 3.49 to 4.9 eV measured by photoluminescence. This results in a tunable 2DEG density from 0 to 3.7×10^{13} cm^2. The room temperature mobilities of $x \geq 0.25$ AlGaN channel HEMTs were limited by alloy disorder scattering to below 50 cm^2/(V.s) for these 2DEG densities, leaving ample room for further heterostructure design improvements to boost mobilities. A characteristic alloy fluctuation energy of ≥1.8 eV for electron scattering in AlGaN alloy is estimated based on the temperature dependent electron transport experiments.

© 2022 Author(s). All article content, except where otherwise noted, is licensed under a Creative Commons Attribution (CC BY) license (http://creativecommons.org/licenses/by/4.0/). https://doi.org/10.1063/5.0121195

Ultra-wide bandgap (UWBG) semiconductor materials have recently been the focus of significant research and technological interest because they offer the possibility of higher-voltage power switching, higher frequency RF electronics, and short-wavelength deep-UV photonics to take electronics and photonics to uncharted territories.[1] This can only be enabled with new semiconductor materials, such as Ga_2O_3, diamond, and AlGaN, that have energy bandgaps much larger than existing semiconductors. Among these, only AlGaN has the unique property of forming conductive channels by polarization-induced doping, which makes it a promising candidate for the future generation of high electron mobility transistors (HEMTs).

Over the past few decades, the GaN-based HEMT has established itself in high-power, high-frequency applications—thanks to its wide bandgap (3.4 eV), high electron velocities (1.4×10^7 cm/s), and ability to form heterostructures exhibiting high carrier mobilities.[2] More recently, AlGaN channel HEMTs based on metal-polar $Al_yGa_{1-y}N/Al_xGa_{1-x}N$ heterostructures with $x < y \leq 1.0$ are being explored for potential advantages over AlGaN/GaN HEMTs.[3,4] Larger critical electric field due to the wider bandgap in AlGaN compared to GaN will enable an increase in output power owing to larger drain voltages that can be sustained in a HEMT based amplifier. This translates directly to a superior Johnson's figure of merit in AlGaN HEMTs, which can be up to four times higher than current GaN HEMTs, making them attractive for high-power RF applications.[5] Khachariya *et al.*[6] recently reported a record high mesa breakdown field of ~11.5 MV/cm in an $Al_{0.85}Ga_{0.15}N/Al_{0.6}Ga_{0.4}N$ HEMT, underscoring the promise of the AlGaN channel for extreme electronics at high voltages and high temperatures. While achieving a wider bandgap channel is desirable, the small conduction band offset between an Al-rich $Al_xGa_{1-x}N$ channel and $Al_yGa_{1-y}N$

© Author(s) 2022

barrier layer can lead to large gate leakage currents. Therefore, for high voltage switching applications where reverse-bias gate leakage is a pressing issue, the AlGaN channel composition needs to be carefully optimized.

Aluminum nitride (AlN) is an emerging platform for mm-wave integrated circuits (MMICs)[7] due to its ultrawide and direct bandgap (6 eV), high thermal conductivity (~340 W/mK), and high piezoelectricity. AlN/GaN/AlN HEMTs[8–12] on this platform, which consist of *thin* and *strained* GaN quantum wells (QWs) hosting 2D electron gases (2DEGs) surrounded by AlN buffer and barrier layers, provide enhanced thermal management and improved breakdown compared to conventional GaN HEMTs. These AlN HEMTs on SiC have recently demonstrated high mm-wave output powers of >3 W/mm at 10 GHz[13] and 2 W/mm at 94 GHz.[14] In this work, we wish to combine the benefits offered by the AlN platform with the merits of an AlGaN channel to realize AlN/AlGaN/AlN double heterostructures and study the physics of polarization induced charges in them. The study of the crystal and electrical transport properties of such structures is needed to determine their potential for applications in RF and power electronics. What is interesting about this AlN/AlGaN/AlN heterostructure is that the whole material stack, consisting of a conductive AlGaN quantum well active region embedded in an insulating AlN matrix, has a very high bandgap, thus enabling access to the highest breakdown electric fields and operating temperatures, beyond the reach of GaN HEMTs.[15,16]

Attaining an ultra-wide bandgap device structure while still having a highly conductive AlGaN channel constitutes a heterostructure design trade-off. For metal-polar AlN/AlGaN/AlN double heterostructures grown along the polar c-axis, the discontinuous electrical polarization $\vec{P}(z)$ across the AlN/AlGaN top interface gives rise to a polarization sheet charge $q\sigma_\pi = -\Delta\vec{P}(z)\cdot\hat{z}$ at that interface. Here, $\Delta\vec{P}(z)$ is the polarization discontinuity at the heterojunction interface, q is the absolute value of the electron charge, and $\hat{z}$ is the unit vector along the growth direction, which in this case is the positive c-axis. AlGaN grown over AlN is under a compressive strain and, thus, has a piezoelectric component of polarization opposing the spontaneous one. Because the top AlN has a higher polarization than $Al_xGa_{1-x}N$ (where x is the Al mole fraction), the net unbalanced bound polarization charge $q\sigma_\pi(x)$ at the AlN/AlGaN interface is positive and decreases with x.[17,18] This positive bound charge creates a high electric field and energy-band bending such that a mobile 2DEG forms at the AlN/AlGaN heterointerface. Similarly, a 2D hole gas (2DHG) should be formed at the bottom AlGaN/AlN interface due to the negative bound charge $-q\sigma_\pi(x)$ present there. Because of its polarization-generated nature, the 2DEG density should electrostatically depend on the thicknesses of the layers and the composition (x) of the AlGaN channel and not on temperature. Furthermore, the conduction band offset $\Delta E_C(x)$ between AlN and $Al_xGa_{1-x}N$, which confines the 2DEG, also decreases with x.[18]

Consequently, for fixed thicknesses of the AlN barrier layer t_b and AlGaN channel layer t_{QW}, the 2DEG density should decrease with increasing Al composition x of the AlGaN channel. This tunability offered by the Al composition for the polarization control of the 2DEG density is of extreme importance in the design space of AlGaN channel polar heterostructures for transistor applications. Abid *et al.*[19] and Maeda *et al.*[20] recently demonstrated the epitaxial growth and promising HEMT device performance of AlN/$Al_{0.5}Ga_{0.5}N$/AlN double heterostructures grown by metalorganic chemical vapor deposition (MOCVD) and pulsed sputtering deposition, respectively. The compositional dependence of 2DEG properties in such AlGaN channel HEMT heterostructures has not been examined yet.

In this work, we report a systematic study of the structural, optical, and electronic transport properties of AlN/AlGaN/AlN double heterostructures with the $Al_xGa_{1-x}N$ channel composition ranging from $x = 0$ to $x = 0.74$, grown using molecular-beam-epitaxy (MBE). Photoluminescence spectra show that the bandgap of the $Al_xGa_{1-x}N$ channel increases with x. Charge control observed in these heterostructures by AlGaN composition tuning agrees well with the polarization model, with 2DEG densities varying from $\sim 3.7 \times 10^{13}$ cm^2 in a GaN channel to no measurable 2DEG in an $Al_{0.74}Ga_{0.26}N$ channel of thickness 24 nm. In addition, temperature-dependent electronic transport measurements reveal that alloy disorder scattering is the dominant scattering mechanism in the AlGaN channel 2DEGs, with an alloy fluctuation potential of ≥1.8 eV for electrons in AlGaN.

AlN/AlGaN/AlN double heterostructures were grown on the Si-face of semi-insulating 6H–SiC substrates using a Veeco GEN10 MBE system equipped with one standard effusion cell for elemental Ga, two cells Al1 and Al2 for elemental Al, and a radio frequency plasma source for the active N species. N plasma power of 400 W, corresponding to a growth rate of 0.42 μm h^{-1}, was used. A 1 μm thick unintentionally doped (UID) AlN buffer layer was epitaxially grown on SiC with a nucleation layer of 50 nm that was grown in a slightly N-rich condition with Al (ϕ_{Al}) to an active N flux (ϕ_N) ratio $\phi_{Al} : \phi_N$ of 0.9, while the remaining 950 nm AlN buffer layer was grown in metal-rich conditions with a $\phi_{Al} : \phi_N$ of 1.1. The N-rich nucleation layer blocks the Si up diffusion from the SiC surface and prevents it from incorporating in the active region.[21,22] This was followed by the growth of $t_{QW} = 24$ nm thick strained AlGaN quantum well to host the 2DEG channel. The Al composition (x) in the $Al_xGa_{1-x}N$ channel was systematically varied from $x = 0$ to $x = 0.74$ (calibrated by x-ray diffraction as discussed later) across six samples by changing the ϕ_{Al} with respect to ϕ_N while keeping the Ga flux (ϕ_{Ga}) constant. The relative flux conditions of $\phi_{Al} + \phi_{Ga} > \phi_N$, $\phi_{Al} < \phi_N$ were maintained to ensure N-limited (or metal-rich) AlGaN MBE growth conditions. An AlN layer of thickness $t_b = 15$ nm was grown on the AlGaN channel as the top barrier. The AlN buffer layer and the top AlN barrier layer were grown using the Al1 cell, whereas the AlGaN channel layer was grown using Al2 cell to avoid growth interrupts. The entire heterostructure was grown at a constant substrate thermocouple temperature of 750 °C. Figure 1(a) shows the schematic layer structures of the AlN/AlGaN/AlN double heterostructures with varying Al content in the AlGaN channel used for this study.

X-ray diffraction (XRD) was used to determine the structural quality of the epitaxial structures and the average Al composition x of the AlGaN channel. Figure 1(b) shows the measured symmetric (002) reflection XRD spectra of the six samples with increasing Al content x, along with the simulated diffraction patterns based on the layer structure shown in Fig. 1(a). The AlGaN peaks are clearly resolved to the left of the substrate SiC peak for all the samples. The clearly visible thickness fringes suggest abrupt hetero-interfaces in the structure. Fitting measured spectra with the simulation

© Author(s) 2022

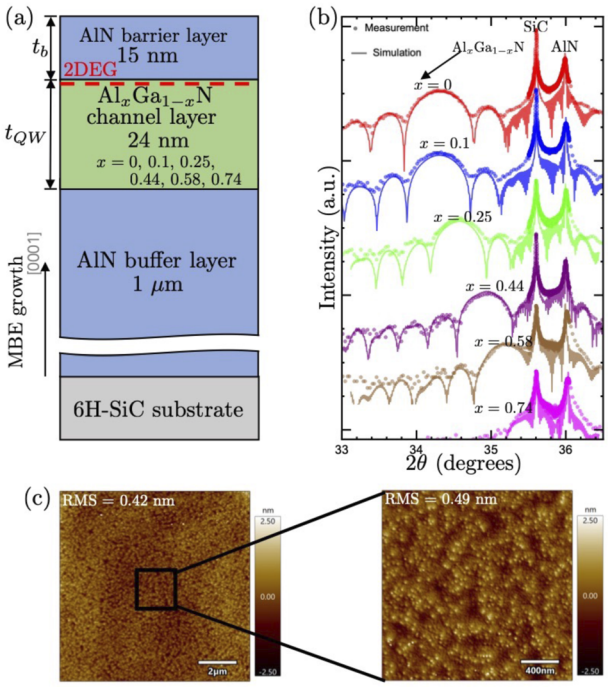

FIG. 1. (a) Schematic and (b) XRD symmetric $\omega/2\theta$ scans of the AlN/Al$_x$Ga$_{1-x}$N/AlN quantum well heterostructures with $0 \le x \le 0.74$. (c) 10×10 and 2×2 μm^2 AFM micrographs of the AlN/Al$_{0.44}$Ga$_{0.56}$N/AlN sample showing smooth surface morphology with sub-nm rms roughness.

confirmed the targeted thickness of the epi-layers while also yielding the average Al mole fraction x in the AlGaN channel layers as 0, 0.1, 0.25, 0.44, 0.58, and 0.74 for the six samples under study. The effect of strain in the AlGaN layer is taken into account to estimate the x values from XRD. All the samples exhibit similar smooth surface morphologies measured by atomic force microscopy (AFM) with rms roughness <0.8 nm over a 10×10 μm^2 area. Figure 1(c) shows a representative AFM scan from the AlN/Al$_{0.44}$Ga$_{0.56}$N/AlN sample.

The in-plane lattice constant of a relaxed wurtzite AlN crystal $a_0^{\mathrm{AlN}} = 3.112$ Å is smaller than that of unstrained Al$_x$Ga$_{1-x}$N $a_0^{\mathrm{AlGaN}} = (3.189 - 0.077x)$ Å, obtained from Vegard's law. Consequently, the c-plane of the AlGaN epitaxial layer grown over AlN experiences an in-plane compressive strain, $\varepsilon_{xx}^{\mathrm{AlGaN}} = (a^{\mathrm{AlGaN}} - a_0^{\mathrm{AlGaN}})/a_0^{\mathrm{AlGaN}}$, where a^{AlGaN} is the lattice constant of the strained AlGaN film on AlN. $\varepsilon_{xx}^{\mathrm{AlGaN}}$ depends both on the Al composition x as well as the thickness of the AlGaN QW layer t_{QW}. Quantification of strain in the AlGaN channel layer is critical for HEMT heterostructure design as it dictates the maximum thickness of the AlN barrier layer that can be grown without cracking.[12] Moreover, it influences the carrier transport properties as it not only determines the piezoelectric polarization, which, in turn, affects the 2DEG carrier density, but also modifies the electron effective mass and, therefore, the mobility.

To experimentally investigate the strain in the AlGaN QW as a function of its Al composition, reciprocal space mapping (RSM) using XRD was conducted on the AlN/AlGaN/AlN heterostructures around the SiC(1 1 12)/AlGaN(1 1 4) peaks to extract the in-plane lattice spacings of the AlGaN layer. RSMs for samples with GaN, Al$_{0.1}$Ga$_{0.9}$N, Al$_{0.25}$Ga$_{0.75}$N, and Al$_{0.44}$Ga$_{0.56}$N QWs are shown in Fig. 2. The extracted a-lattice constants are $a^{\mathrm{AlN}} = 3.1089$ Å for the AlN buffer layer and $a^{\mathrm{GaN}} = 3.1230$ Å, $a^{\mathrm{Al_{0.1}Ga_{0.9}N}} = 3.1160$ Å, $a^{\mathrm{Al_{0.25}Ga_{0.75}N}} = 3.1135$ Å, and $a^{\mathrm{Al_{0.44}Ga_{0.56}N}} = 3.1089$ Å for the various strained AlGaN QW layers. With increasing Al composition, the maximum reflection intensity of AlGaN reciprocal lattice points (RLPs) progressively shifts from a partially relaxed $(0 < R < 1)$ toward a fully strained $(R = 0)$ position, as seen in Fig. 2. Here, the degree of relaxation $R = (a^{\mathrm{AlGaN}} - a^{\mathrm{AlN}})/(a_0^{\mathrm{AlGaN}} - a^{\mathrm{AlN}})$ is calculated with respect to the AlN buffer layer. As the QW changes from GaN to Al$_{0.44}$Ga$_{0.56}$N, the AlGaN layer becomes more

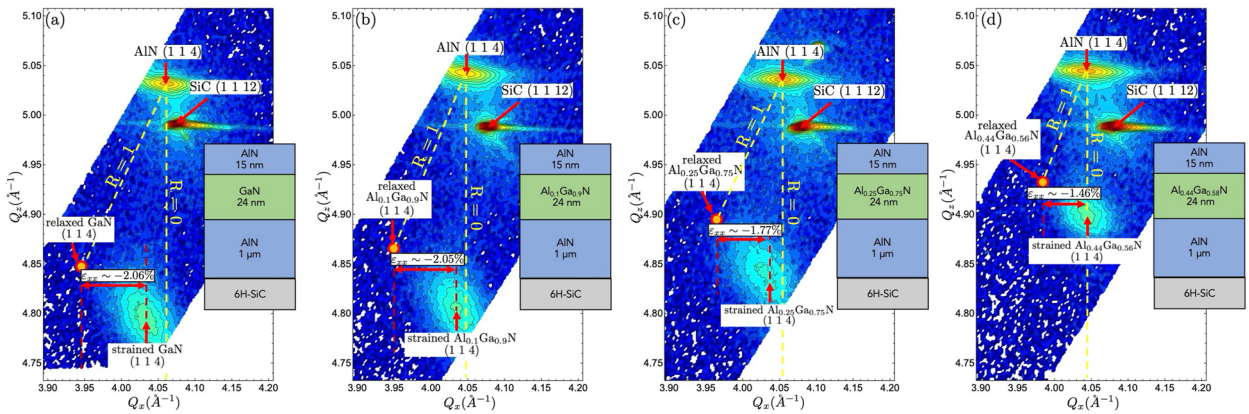

FIG. 2. Asymmetric RSM scans of AlN/Al$_x$Ga$_{1-x}$N/AlN samples with (a) GaN, (b) Al$_{0.1}$Ga$_{0.9}$N, (c) Al$_{0.25}$Ga$_{0.75}$N, and (d) Al$_{0.44}$Ga$_{0.56}$N quantum well channel layers. The dashed yellow lines indicate where the fully relaxed $(R = 1)$ and fully strained $(R = 0)$ Al$_x$Ga$_{1-x}$N layers with varying Al compositions should be. The Al$_x$Ga$_{1-x}$N RLPs get closer to the fully strained position with increasing x. The in-plane compressive strain (ε_{xx}) in the AlGaN layers, extracted with respect to their relaxed (114) position, decreases as the AlGaN layer gets more Al-rich.

© Author(s) 2022

pseudomorphic and assumes the in-plane lattice constants of the underlying AlN layer. The signal from the top AlN barrier in the RSM is aliased by the stronger signal from the bottom AlN buffer layer.

The compositional dependence of the extracted strain ε_{xx} and the relaxation R in the AlGaN QW are shown in Fig. 3. Data from other AlN/AlGaN/AlN samples with $Al_{0.58}Ga_{0.42}N$ and $Al_{0.74}Ga_{0.26}N$ QW are also included. It is clearly seen that both the strain and the relaxation of the AlGaN QW decrease as x increases. The strain shows a monotonic reduction, while the relaxation drops to 0 for $x \geq 0.44$. The dashed gray line in Figs. 3(a) and 3(b) show the theoretical dependence of ε_{xx} and R with x if the AlGaN layer is grown pseudomorphically to the AlN buffer. These results indicate that higher composition ($x \geq 0.44$) AlGaN QW can be grown even thicker than 24 nm over AlN without significant relaxation, opening up opportunities for further improvements in the heterostructure design. In addition, the screw threading dislocation densities in the samples were estimated from the full width at half maximum (FWHM) values of the x-ray rocking curves (XRCs) along the AlGaN(0002) plane. The GaN QW sample has a screw dislocation density of ~1.6×10^9 cm^2, which decreases to ~1.1×10^8 cm^2 for the $Al_{0.74}Ga_{0.26}N$ QW sample.

Figure 4 shows the 300 K photoluminescence (PL) spectra of the AlN/AlGaN/AlN double heterostructures with varying Al composition of the QW. The GaN QW sample was excited by a 325 nm He–Cd laser, whereas the rest of the AlGaN QW samples were excited by a 193 nm ArF excimer laser. Band-to-band PL emission from the AlGaN QW is observed for all six samples. The AlGaN QW PL peaks at 355 nm (3.49 eV), 340 nm (3.64 eV), 325 nm (3.81 eV), 289 nm (4.29 eV), 273 nm (4.54 eV), and 253 nm (4.9 eV) for the GaN, $Al_{0.1}Ga_{0.9}N$, $Al_{0.25}Ga_{0.75}N$, $Al_{0.44}Ga_{0.56}N$, $Al_{0.58}Ga_{0.42}N$, and $Al_{0.74}Ga_{0.26}N$ QW samples, respectively. It is evident that as the Al composition x of the QW channel increases, the interband transition PL peak blue-shifts, giving a direct signature of the increasing bandgap of the channel. This also shows the tunability of the bandgap of the AlGaN channel layer between GaN and AlN. The predicted energy gap values for x = 0, 0.1, 0.25, 0.44, 0.58, and 0.74 are 3.42, 3.61, 3.94, 4.43, 4.83, and 5.34 eV, respectively,

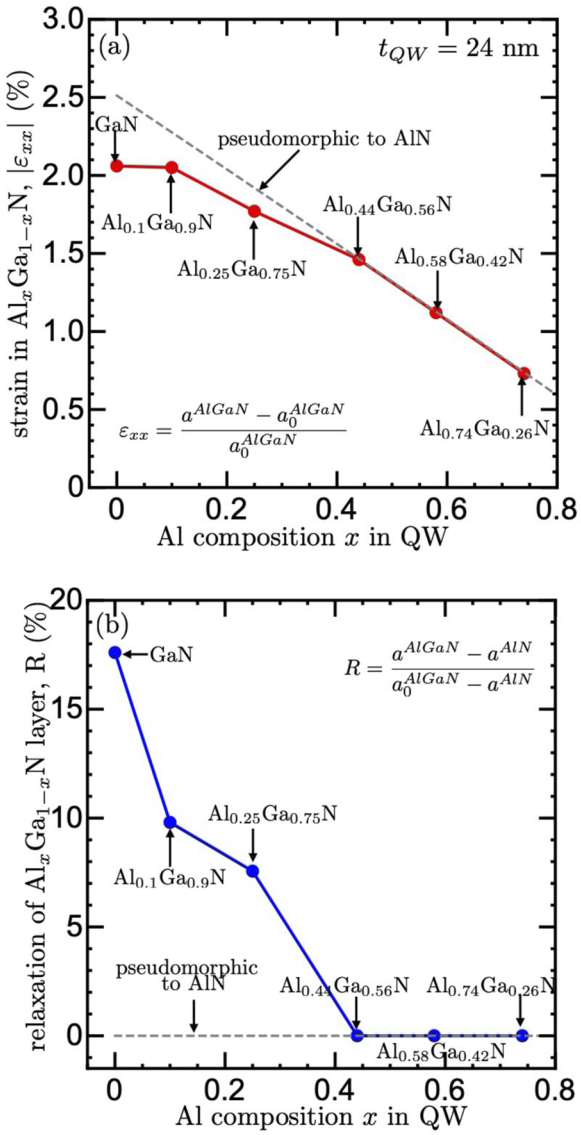

FIG. 3. Experimental dependence of the (a) in-plane compressive strain ε_{xx} and (b) relaxation R in the AlGaN layer as a function of the Al concentration x in the MBE-grown AlN/AlGaN/AlN heterostructure grown on 6-H SiC. ε_{xx} and R are extracted from x-ray diffraction reciprocal space maps shown in Fig. 2. ε_{xx} is calculated with respect to the relaxed AlGaN in-plane lattice constant (a_0^{AlGaN}), and R is calculated with respect to the AlN buffer layer lattice constant (a^{AlN}). The dashed gray lines indicate the theoretical compositional dependence of ε_{xx} and R in AlGaN QW layers fully strained to the underlying AlN buffer layer.

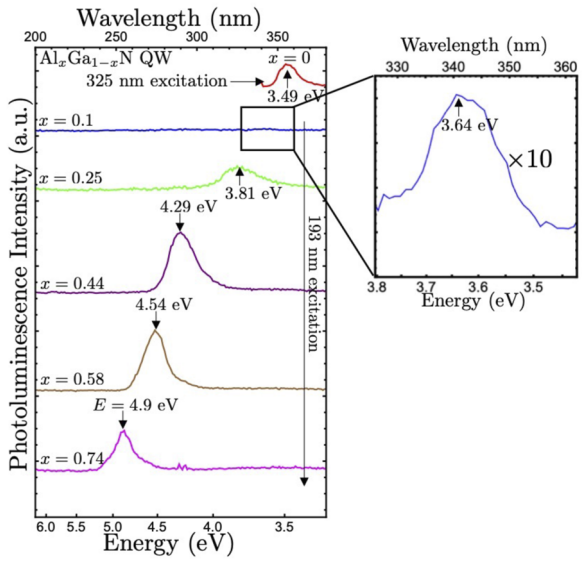

FIG. 4. Photoluminescence spectra of AlN/AlGaN/AlN double heterostructures with varying Al composition x of the AlGaN QW at T = 300 K, showing photon emission from the AlGaN QWs. The PL intensity of the $Al_{0.1}Ga_{0.9}N$ QW sample was multiplied by a factor of 10 in the inset to show the emission peak clearly.

© Author(s) 2022

taking into account a bowing parameter of 1 eV.[23] The difference between the measured and predicted values, specifically the PL peak broadening, intensity suppression, and peak shifts, are attributed to properties including a variability in optical absorption coefficient, quantum confinement, strain, compositional fluctuation, and polarization-induced quantum-confined Stark effect (QCSE).

Thus, the AlN/AlGaN/AlN samples have the desired structures in which the electrical transport properties of 2DEGs can be studied systematically as a function of Al composition x. As discussed previously, the sheets of charge $\pm q\sigma_{\pi}(x)$, located at the AlN/AlGaN heterointerfaces, induce a rearrangement of free carriers. Theoretically, this rearrangement generates a 2DEG at the top interface and a 2DHG at the bottom one. A self-consistent 1D Schrödinger–Poisson energy band diagram simulation for the heterostructures under study is shown in Fig. 5(a) for three samples with GaN, $Al_{0.44}Ga_{0.56}N$, and $Al_{0.74}Ga_{0.26}N$ QW channels, with a surface barrier height $q\phi_B$ = 2.2 eV. With increasing Al concentration x, the bandgap inside the QW widens, thereby pushing up the conduction band edge E_C with respect to the Fermi level E_F. The 2DEG density decreases commensurately with increasing x. Eventually, as shown in Fig. 5(a), E_F should move into the bandgap, as is the case for $Al_{0.74}Ga_{0.26}N$ QW channel. At and beyond that x, there should be no 2DEG in an as-grown heterostructure for the given layer thicknesses.

Hall-effect measurements were performed on the samples using soldered corner indium contacts to the AlGaN QW 2DEGs. The results of the Hall-effect measurements are summarized in Table I. All the samples except the one with $Al_{0.74}Ga_{0.26}N$ QW showed Hall conductivity, indicating the presence of 2DEGs. As discussed earlier, the polarization induced 2DEG is most likely absent in the $Al_{0.74}Ga_{0.26}N$ QW sample as the polarization difference between the top AlN and $Al_{0.74}Ga_{0.26}N$ layers is not large enough to induce the 2DEG for the given thicknesses of the layers. No direct evidence of the 2DHG formed at the bottom AlGaN/AlN interface was observed in the Hall-effect measurements for the samples reported here. Figure 5(b) compares the experimentally measured 2DEG Hall densities in the AlN/AlGaN/AlN samples to the simulated 2DEG densities n_s from a self-consistent 1D Schrödinger–Poisson calculation. The 2DEG densities $n_s(x)$ are calculated as a function of AlGaN channel composition x for different surface barrier heights $q\phi_B$ of 1.2, 2.2, and 3 eV. As the Al mole fraction in the channel increases, the measured 2DEG density decreases from 3.78×10^{13} cm^2 in the GaN channel to the $Al_{0.74}Ga_{0.26}N$ channel sample, which shows no 2DEG, in agreement with the simulated results. A surface barrier height of $q\phi_B$ = 2.2 eV results in the best fit to the experimental data. The surface Fermi level is not pinned in AlN and a fixed surface barrier height $q\phi_B$ may not necessarily explain the experimental data well over the entire range of samples with varying Al composition x in the AlGaN QW channel. For AlGaN/GaN HEMTs, it has been previously observed that $q\phi_B$ is dependent on carrier concentration[24] and the AlGaN barrier thickness.[25] The unpinned surface Fermi level in the AlN barrier layer presents an attractive opportunity to employ work function engineering to tune threshold voltages of transistors.

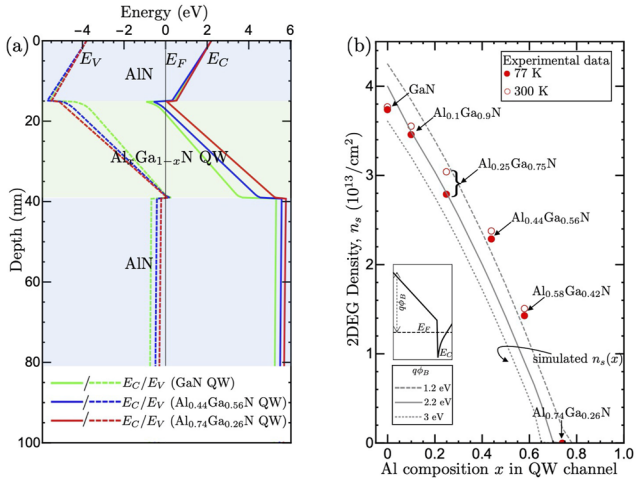

FIG. 5. (a) 1D Schrödinger–Poisson energy band diagram simulation showing the control of the as-grown 2DEG in the AlGaN channel by adjusting the Al composition in the channel. Green curve is the GaN channel, blue curve is the $Al_{0.44}Ga_{0.56}N$ channel, and red curve is the $Al_{0.74}Ga_{0.26}N$ channel. (b) Measured 2DEG Hall densities at 77 K (filled circles) and 300 K (hollow circles) as a function of Al composition x in the AlGaN QW channel for different samples. The simulated 2DEG densities (gray lines) are also plotted as a function of Al composition for different surface barrier heights $q\phi_B$ (inset) and show good agreement with the experimental data.

TABLE I. Structural details of the AlN/AlGaN/AlN double-heterostructures studied in this work, with the corresponding bandgap of the AlGaN channel measured via photoluminescence and their 2DEG densities n_s and mobilities μ measured via Hall-effect at 300 and 77 K. A sheet resistance R_s of $>10^3$ kΩ per sq. indicates resistive samples in which the transport could not be extracted using Hall effect measurements.

Channel layer	Energy bandgap from PL (eV)	$n_s^{300\,K}$ (10^{13} cm^2)	μ^{300K} [cm^2/(V.s)]	$R_s^{300\,K}$ (kΩ per sq.)	$n_s^{77\,K}$ (10^{13} cm^2)	μ^{77K} [cm^2/(V.s)]	$R_s^{77\,K}$ (kΩ per sq.)
GaN	3.49	3.78	401	0.41	3.75	614	0.27
$Al_{0.1}Ga_{0.9}N$	3.64	3.56	250	0.7	3.47	355	0.5
$Al_{0.25}Ga_{0.75}N$	3.81	3.05	45	4.55	2.8	52	4.29
$Al_{0.44}Ga_{0.56}N$	4.29	2.39	36	7.26	2.3	33	8.23
$Al_{0.58}Ga_{0.42}N$	4.54	1.52	24	17.13	1.44	21	20.66
$Al_{0.74}Ga_{0.26}N$	4.9	⋯	⋯	$>10^3$	⋯	⋯	$>10^3$

© Author(s) 2022

A good electrostatic control over the 2DEG densities is thus demonstrated by varying the Al composition of the AlGaN layer in as-grown heterostructures. The higher the Al composition x, the higher the AlGaN channel bandgap and hence higher the expected electrical breakdown field. However, the 2DEG density decreases with an increase in x. A high 2DEG density is desired in RF HEMTs to obtain high on-currents and low access resistances. Hence, this trade-off between channel breakdown and on-current needs to be carefully optimized for designing an AlGaN-channel HEMT. This study, therefore, provides valuable experimental data for guiding the heterostructure and device design for AlGaN-channel HEMTs for high-power, high-frequency applications.

It is worth mentioning here that even though the as-grown heterostructure with the $Al_{0.74}Ga_{0.26}N$ channel is highly resistive, it can potentially enable normally off operation with high threshold voltage, which is desirable for power switching and energy conversion applications. Previous reports[26,27] have theoretically simulated the enhancement mode operation in such high composition AlGaN HEMTs; however, the experimental demonstration of such devices remains to be realized yet. Clever device engineering would be needed to alleviate the effects of increased access region resistance originating from the reduced polarization difference between the barrier and channel in such E-mode HEMTs. As an example, selective-area ion implantation of Si in the access region of the AlGaN channel could help solve this problem.

A temperature-dependent electron transport study was performed for all the AlGaN QW channel samples that showed conductivity. Figures 6(a) and 6(b) show the temperature-dependent Hall-effect measurement results from 300 K down to 10 K. In all samples, the 2DEG density does not show significant variation with temperature. This robustness of the 2DEG densities with temperature confirms their polarization-induced origin.

The electron mobility in the GaN and $Al_{0.1}Ga_{0.9}N$ QW channel samples increases monotonically upon lowering the temperature, as expected due to freeze-out of phonon scattering. However, due to additional alloy scattering, the 10 K mobility in $Al_{0.1}Ga_{0.9}N$ QW is limited to ~360 $cm^2/(V.s)$ compared to ~630 $cm^2/(V.s)$ in GaN QW. The rest of the samples with $Al_{0.25}Ga_{0.75}N$, $Al_{0.44}Ga_{0.56}N$, and $Al_{0.58}Ga_{0.42}N$ channels show nearly constant mobilities $\lesssim 50$ $cm^2/(V.s)$ over the whole temperature range, indicating that temperature independent alloy scattering is the dominant scattering mechanism. Other scattering mechanisms, such as dislocation scattering, surface charge scattering and interface roughness scattering, were found to be much weaker than alloy scattering in the AlGaN channel for the whole temperature range.

The mobilities of MBE-grown $x \geq 0.25$ AlGaN channel HEMTs in this study are lower than the values reported previously in MOCVD-grown high Al composition AlGaN channel HEMT structures.[28–30] For example, Baca *et al.*[29] measured a mobility of 250 $cm^2/(V.s)$ in $AlN/Al_{0.85}Ga_{0.15}N$ HEMT for a carrier density of 6×10^{12} cm^2, and Xue *et al.*[30] reported a mobility of 175 $cm^2/(V.s)$ for a carrier density of 8.5×10^{12} cm^2 in the $Al_{0.75}Ga_{0.25}N/Al_{0.6}Ga_{0.4}N$ HEMT structure. The observation of lower carrier mobilities in our films may partly be attributed to higher alloy scattering due to comparatively higher electron densities in our HEMT heterostructures. It is also possible that the MBE-grown AlGaN films in the current study suffer from relatively higher lateral alloy fluctuations, hence causing AlN/GaN energy barriers for lateral electron transport.[31]

For electrons in the AlGaN QW, the mobility decreases with the increasing Al composition (decreasing by up to 90% in higher composition AlGaN compared to GaN) due to the combined effects of alloy scattering and the increase in the Γ valley conduction band edge electron effective mass. Quantitatively, under a single parabolic conduction band approximation, the alloy disorder limited mobility μ_{alloy} of 2D electron carriers in an alloy channel with composition x is given by[32]

$$\mu_{alloy}(n_s, x) \approx \frac{q\hbar^3}{m^*(x)^2 \Omega_0(x) U_{AL}^2 x(1-x)} \cdot \frac{16}{3b(n_s(x), x)}, \quad (1)$$

where $\hbar$ is the reduced Planck's constant and $m^*(x)$ is the effective mass of electrons in AlGaN of composition x, interpolated between the Γ valley effective mass of GaN ($0.2m_0$) and AlN ($0.4m_0$), where m_0 is the free electron effective mass. $b(n_s, x) = [(33m^*(x)q^2 n_s)/(8\hbar^2 \varepsilon_0 \varepsilon_s)]^{1/3}$ is the variational Fang–Howard wavefunction parameter that quantifies the spatial spread of the 2DEG. $\Omega_0(x) = \sqrt{3}/2 \cdot a_0^{AlGaN}(x)^2 c_0^{AlGaN}(x)$ is the volume of the

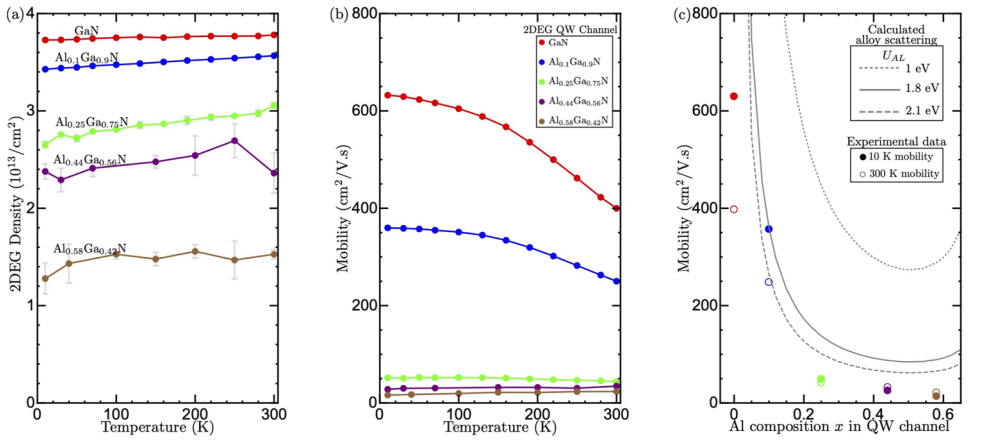

FIG. 6. Temperature dependent (a) measured 2DEG Hall densities and (b) measured 2DEG Hall mobilities for samples with varying Al composition in the AlGaN QW channel. (c) 10 K (filled circle) and 300 K (hollow circle) electron mobilities as a function of Al composition x in the AlGaN QW channel. The gray curves show that the calculated alloy scattering mobilities for different alloy scattering potentials confirm that the major scattering mechanism in high Al composition AlGaN channel 2DEGs is alloy scattering. Color scheme for the plots shown in (b) is the same across the panels for different samples.

© Author(s) 2022

wurtzite unit cell, where a_0^{AlGaN} and c_0^{AlGaN} are the interpolated in-plane and out-of-plane lattice constants of AlGaN. U_{AL} is the alloy fluctuation potential and is typically estimated by fitting to experimental mobility measurements. In the absence of experimental data, U_{AL} is approximated to be the conduction band offset ΔE_C or bandgap difference ΔE_g between the constituents of the ternary alloy,[33,34] which in our case are GaN and AlN. For AlGaN, U_{AL} has been estimated to be between 1.3 and 2.2 eV by various theoretical and experimental methods.[34–38] The series of polarization induced, undoped AlN/AlGaN/AlN 2DEG samples used in this study offer an opportunity to quantify U_{AL} for AlGaN to understand the physical limits of 2DEG mobilities in AlGaN channel HEMTs.

Using Eq. (1), μ_{alloy} is calculated for AlN/Al_xGa_{1-x}N/AlN heterostructures as a function of Al content x = 0–0.8 for various short-range alloy scattering potentials U_{AL} = 1, 1.8 and 2.1 eV. For mobility calculations, $n_s(x)$ is obtained from the 1D Schrödinger–Poisson solver using a surface barrier height $q\phi_B$ of 2.2 eV, as discussed earlier in Fig. 5(b). The results of calculated μ_{alloy} are plotted in Fig. 6(c) along with the measured 10 and 300 K Hall mobilities in the AlN/AlGaN/AlN samples as a function of Al composition x. Compositional dependence of the measured 10 K mobilities in the AlGaN channel fall on U-shaped curve characteristic of alloy scattering. Upon comparing experimental data with calculated μ_{alloy} [gray curves in Fig. 6(c)], it is predicted that $U_{AL} \gtrsim 1.8$ eV. It should be noted that the 2DEG mobilities in these AlN/AlGaN/AlN double heterostructures could have been adversely affected by the 2DHG formed at the bottom AlGaN/AlN heterojunction due to proximity phenomena, such as Coulomb drag effect, as has been suspected earlier for AlN/GaN/AlN heterostructures.[8,9]

Thus, the low-field mobility in AlGaN channel 2DEGs is a strong function of alloy composition, and it degrades with increasing Al composition x. How do we increase the mobilities of these 2DEGs? Since the mobility in the AlGaN channel is intrinsically bound by the limits set by the statistical disorder in the alloy system, the low-field conductivity in such alloyed channels can be potentially boosted by switching to a $(GaN)_n/(AlN)_m$ "digital alloy" scheme. Such a superlattice alloying method for the AlGaN-channel has been recently proposed theoretically by Pant *et al.*[39] to diminish the in-plane disorder scattering while still maintaining the high breakdown characteristics. The mobility is also expected to improve by moving to bulk single-crystal AlN substrates, which have less defects and dislocations compared to AlN films grown on foreign substrates, such as Si, SiC, and sapphire. Recently, high quality AlN homoepitaxy has been demonstrated both on the Al-face[40,41] and N-face[42] of native AlN substrates, which can enable further advancements in AlGaN channel HEMTs. Finally, most of the work to date has been focused on metal-polar AlGaN channel transistors. The N-polar AlGaN/AlN heterostructure, which unlike the metal-polar AlN/AlGaN/AlN heterostructure hosts a 2DEG in the AlGaN channel *without* an accompanying 2DHG, offers the possibility of even further mobility enhancement.

In summary, this work presents a systematic study of MBE-grown AlN/AlGaN/AlN double heterostructures with thin and strained $Al_xGa_{1-x}N$ quantum well channels surrounded by AlN. The material characteristics of the heterostructures and the transport properties of the 2DEGs in AlGaN channels have been examined as a function of the Al composition $0 \le x \le 0.74$. Photon emission from the AlGaN QWs was observed in the photoluminescence spectra. The bandgap increased with x ranging from 3.49 to 4.9 eV. The density of the 2DEG could be manipulated from 0 to 3.7×10^{13} cm^2 by changing x while keeping the thicknesses of the layers constant. Thus, these AlGaN channel HEMT heterostructures lay the groundwork for new generations of high-power RF and mm-wave HEMTs. These structures would also be useful for pushing the breakdown voltages higher for power switching applications. More importantly, the AlN platform allows for the integration of nitride RF and mm-wave amplifiers with components, such as p-channel FETs, and RF and mm-wave filters as described by Hickman *et al.*[7]

The authors thank Jimy Encomendero, Yongjin Cho, John Wright, and Len van Deurzen for useful discussions. This work was supported by the Cornell Center for Materials Research (CCMR)—a NSF MRSEC program (Grant No. DMR-1719875); ULTRA, an Energy Frontier Research Center funded by the U.S. Department of Energy (DOE), Office of Science, Basic Energy Sciences (BES), under Award No. DE-SC0021230; AFOSR Grant No. FA9550-20-1-0148; and the Semiconductor Research Corporation (SRC) Joint University Microelectronics Program (JUMP). This work uses the Cornell Nanoscale Facilities, supported by NSF Grant No. NNCI-202523 and CESI Shared Facilities partly sponsored by NSF Grant No. MRI DMR-1631282 and Kavli Institute at Cornell (KIC).

AUTHOR DECLARATIONS

Conflict of Interest

The authors have no conflicts to disclose.

Author Contributions

Jashan Singhal: Conceptualization (lead); Data curation (lead); Formal analysis (lead); Investigation (lead); Methodology (lead); Writing – original draft (lead); Writing – review & editing (lead). **Reet Chaudhuri**: Formal analysis (supporting); Investigation (supporting); Writing – review & editing (supporting). **Austin Hickman**: Investigation (supporting). **Vladimir Protasenko**: Investigation (supporting). **Huili Grace Xing**: Funding acquisition (equal); Project administration (equal); Resources (equal); Supervision (equal); Validation (equal). **Debdeep Jena**: Conceptualization (equal); Funding acquisition (equal); Investigation (equal); Methodology (equal); Project administration (equal); Supervision (equal); Validation (equal); Visualization (equal); Writing – original draft (lead); Writing – review & editing (lead).

DATA AVAILABILITY

The data that support the findings of this study are available from the corresponding author upon reasonable request.

REFERENCES

[1] J. Y. Tsao, S. Chowdhury, M. A. Hollis, D. Jena, N. M. Johnson, K. A. Jones, R. J. Kaplar, S. Rajan, C. G. Van de Walle, E. Bellotti, C. L. Chua, R. Collazo, M. E. Coltrin, J. A. Cooper, K. R. Evans, S. Graham, T. A. Grotjohn, E. R. Heller, M. Higashiwaki, M. S. Islam, P. W. Juodawlkis, M. A. Khan, A. D. Koehler, J. H. Leach, U. K. Mishra, R. J. Nemanich, R. C. N. Pilawa-Podgurski, J. B.

© Author(s) 2022

Shealy, Z. Sitar, M. J. Tadjer, A. F. Witulski, M. Wraback, and J. A. Simmons, "Ultrawide-bandgap semiconductors: Research opportunities and challenges," Adv. Electron. Mater. **4**, 1600501 (2018).
[2]U. K. Mishra, L. Likun, T. E. Kazior, and Y.-F. Wu, "GaN-based RF power devices and amplifiers," Proc. IEEE **96**, 287–305 (2008).
[3]R. J. Kaplar, A. A. Allerman, A. M. Armstrong, M. H. Crawford, J. R. Dickerson, A. J. Fischer, A. G. Baca, and E. A. Douglas, "Review—Ultra-wide-bandgap AlGaN power electronic devices," ECS J. Solid State Sci. Technol. **6**, Q3061–Q3066 (2016).
[4]A. G. Baca, A. M. Armstrong, B. A. Klein, A. A. Allerman, E. A. Douglas, and R. J. Kaplar, "Al-rich AlGaN based transistors," J. Vac. Sci. Technol. A **38**, 020803 (2020).
[5]M. E. Coltrin, A. G. Baca, and R. J. Kaplar, "Analysis of 2D transport and performance characteristics for lateral power devices based on AlGaN alloys," ECS J. Solid State Sci. Technol. **6**, S3114–S3118 (2017).
[6]D. Khachariya, S. Mita, P. Reddy, S. Dangi, J. H. Dycus, P. Bagheri, M. H. Breckenridge, R. Sengupta, S. Rathkanthiwar, R. Kirste, E. Kohn, Z. Sitar, R. Collazo, and S. Pavlidis, "Record >10 MV/cm mesa breakdown fields in $Al_{0.85}Ga_{0.15}N/Al_{0.6}Ga_{0.4}N$ high electron mobility transistors on native AlN substrates," Appl. Phys. Lett. **120**, 172106 (2022).
[7]A. L. Hickman, R. Chaudhuri, S. J. Bader, K. Nomoto, L. Li, J. C. M. Hwang, H. Grace Xing, and D. Jena, "Next generation electronics on the ultrawide-bandgap aluminum nitride platform," Semicond. Sci. Technol. **36**, 044001 (2021).
[8]G. Li, B. Song, S. Ganguly, M. Zhu, R. Wang, X. Yan, J. Verma, V. Protasenko, H. Grace Xing, and D. Jena, "Two-dimensional electron gases in strained quantum wells for AlN/GaN/AlN double heterostructure field-effect transistors on AlN," Appl. Phys. Lett. **104**, 193506 (2014).
[9]M. Qi, G. Li, S. Ganguly, P. Zhao, X. Yan, J. Verma, B. Song, M. Zhu, K. Nomoto, H. Xing, and D. Jena, "Strained GaN quantum-well FETs on single crystal bulk AlN substrates," Appl. Phys. Lett. **110**, 063501 (2017).
[10]A. Hickman, R. Chaudhuri, S. J. Bader, K. Nomoto, K. Lee, H. G. Xing, and D. Jena, "High breakdown voltage in RF AlN/GaN/AlN quantum well HEMTs," IEEE Electron Device Lett. **40**, 1293–1296 (2019).
[11]S. Patwal, M. Agrawal, K. Radhakrishnan, T. L. A. Seah, and N. Dharmarasu, "Enhancement of 2D electron gas mobility in an AlN/GaN/AlN double-heterojunction high-electron-mobility transistor by epilayer stress engineering," Phys. Status Solidi A **217**, 1900818 (2020).
[12]R. Chaudhuri, A. Hickman, J. Singhal, J. Casamento, H. G. Xing, and D. Jena, "In situ crystalline AlN passivation for reduced RF dispersion in strained-channel AlN/GaN/AlN high-electron-mobility transistors," Phys. Status Solidi A **219**, 2100452 (2022).
[13]A. Hickman, R. Chaudhuri, L. Li, K. Nomoto, S. J. Bader, J. C. Hwang, H. G. Xing, and D. Jena, "First RF power operation of AlN/GaN/AlN HEMTs with >3 A/mm and 3 W/mm at 10 GHz," IEEE J. Electron Devices Soc. **9**, 121–124 (2020).
[14]A. Hickman, R. Chaudhuri, N. Moser, M. Elliott, K. Nomoto, L. Li, J. C. M. Hwang, H. Grace Xing, and D. Jena, "Large signal response of AlN/GaN/AlN HEMTs at 30 GHz," in *2021 Device Research Conference (DRC)* (IEEE, Piscataway, NJ, 2021), pp. 1–2.
[15]F. Medjdoub, J.-F. Carlin, M. Gonschorek, E. Feltin, M. Py, D. Ducatteau, C. Gaquiere, N. Grandjean, and E. Kohn, "*Can InAlN/GaN be an alternative to high power/high temperature AlGaN/GaN devices?*," in *2006 International Electron Devices Meeting* (IEEE, Piscataway, NJ, 2006), pp. 1–4.
[16]D. Maier, M. Alomari, N. Grandjean, J.-F. Carlin, M.-A. Diforte-Poisson, C. Dua, S. Delage, and E. Kohn, "InAlN/GaN HEMTs for operation in the 1000 °C regime: A first experiment," IEEE Electron Device Lett. **33**, 985–987 (2012).
[17]O. Ambacher, J. Smart, J. R. Shealy, N. G. Weimann, K. Chu, M. Murphy, W. J. Schaff, L. F. Eastman, R. Dimitrov, L. Wittmer, M. Stutzmann, W. Rieger, and J. Hilsenbeck, "Two-dimensional electron gases induced by spontaneous and piezoelectric polarization charges in N- and Ga-face AlGaN/GaN heterostructures," J. Appl. Phys. **85**, 3222–3233 (1999).
[18]C. Wood and D. Jena, *Polarization Effects in Semiconductors: From Ab Initio Theory to Device Applications* (Springer Science & Business Media, 2007).
[19]I. Abid, J. Mehta, Y. Cordier, J. Derluyn, S. Degroote, H. Miyake, and F. Medjdoub, "AlGaN channel high electron mobility transistors with regrown ohmic contacts," Electronics **10**, 635 (2021).
[20]R. Maeda, K. Ueno, A. Kobayashi, and H. Fujioka, "$AlN/Al_{0.5}Ga_{0.5}N$ HEMTs with heavily Si-doped degenerate GaN contacts prepared via pulsed sputtering," Appl. Phys. Express **15**, 031002 (2022).
[21]C. Poblenz, P. Waltereit, S. Rajan, U. K. Mishra, J. S. Speck, P. Chin, I. Smorchkova, and B. Heying, "Effect of AlN nucleation layer growth conditions on buffer leakage in AlGaN/GaN high electron mobility transistors grown by molecular beam epitaxy (MBE)," J. Vac. Sci. Technol. B **23**, 1562–1567 (2005).
[22]W. E. Hoke, A. Torabi, J. J. Mosca, R. B. Hallock, and T. D. Kennedy, "Rapid silicon outdiffusion from SiC substrates during molecular-beam epitaxial growth of AlGaN/GaN/AlN transistor structures," J. Appl. Phys. **98**, 084510 (2005).
[23]F. Yun, M. A. Reshchikov, L. He, T. King, H. Morkoç, S. W. Novak, and L. Wei, "Energy band bowing parameter in $Al_xGa_{1-x}N$ alloys," J. Appl. Phys. **92**, 4837–4839 (2002).
[24]K. Köhler, S. Müller, R. Aidam, P. Waltereit, W. Pletschen, L. Kirste, H. P. Menner, W. Bronner, A. Leuther, R. Quay, M. Mikulla, O. Ambacher, R. Granzner, F. Schwierz, C. Buchheim, and R. Goldhahn, "Influence of the surface potential on electrical properties of $Al_xGa_{1-x}N/GaN$ heterostructures with different Al-content: Effect of growth method," J. Appl. Phys. **107**, 053711 (2010).
[25]G. Li, Y. Cao, H. G. Xing, and D. Jena, "High mobility two-dimensional electron gases in nitride heterostructures with high Al composition AlGaN alloy barriers," Appl. Phys. Lett. **97**, 222110 (2010).
[26]H. Hahn, B. Reuters, H. Kalisch, and A. Vescan, "AlN barrier HFETs with AlGaN channels to shift the threshold voltage to higher positive values: A proposal," Semicond. Sci. Technol. **28**, 074017 (2013).
[27]S. Bajaj, T.-H. Hung, F. Akyol, D. Nath, and S. Rajan, "Modeling of high composition AlGaN channel high electron mobility transistors with large threshold voltage," Appl. Phys. Lett. **105**, 263503 (2014).
[28]A. G. Baca, B. A. Klein, J. R. Wendt, S. M. Lepkowski, C. D. Nordquist, A. M. Armstrong, A. A. Allerman, E. A. Douglas, and R. J. Kaplar, "RF performance of $Al_{0.85}Ga_{0.15}N/Al_{0.70}Ga_{0.30}N$ high electron mobility transistors with 80-nm gates," IEEE Electron Device Lett. **40**, 17–20 (2019).
[29]A. G. Baca, A. M. Armstrong, A. A. Allerman, E. A. Douglas, C. A. Sanchez, M. P. King, M. E. Coltrin, T. R. Fortune, and R. J. Kaplar, "An $AlN/Al_{0.85}Ga_{0.15}N$ high electron mobility transistor," Appl. Phys. Lett. **109**, 033509 (2016).
[30]H. Xue, C. H. Lee, K. Hussian, T. Razzak, M. Abdullah, Z. Xia, S. H. Sohel, A. Khan, S. Rajan, and W. Lu, "$Al_{0.75}Ga_{0.25}N/Al_{0.6}Ga_{0.4}N$ heterojunction field effect transistor with f_T of 40 GHz," Appl. Phys. Express **12**, 066502 (2019).
[31]S. Bajaj, "Design and engineering of AlGaN channel-based transistors," Ph.D. thesis, The Ohio State University, 2018.
[32]G. Bastard, *Wave Mechanics Applied to Semiconductor Heterostructures* (Wiley-Interscience, Hoboken, NJ, 1988).
[33]J. W. Harrison and J. R. Hauser, "Theoretical calculations of electron mobility in ternary III-V compounds," J. Appl. Phys. **47**, 292–300 (1976).
[34]E. Bellotti, F. Bertazzi, and M. Goano, "Alloy scattering in AlGaN and InGaN: A numerical study," J. Appl. Phys. **101**, 123706 (2007).
[35]D. Jena, S. Heikman, J. S. Speck, A. Gossard, U. K. Mishra, A. Link, and O. Ambacher, "Magnetotransport properties of a polarization-doped three-dimensional electron slab in graded AlGaN," Phys. Rev. B **67**, 153306 (2003).
[36]J. Simon, A. Wang, H. Xing, S. Rajan, and D. Jena, "Carrier transport and confinement in polarization-induced three-dimensional electron slabs: Importance of alloy scattering in AlGaN," Appl. Phys. Lett. **88**, 042109 (2006).
[37]M. Miyoshi, S. Fujita, and T. Egawa, "Numerical and experimental analyses of two-dimensional electron mobility in Al(In, Ga)N/AlGaN heterostructures," Appl. Phys. Express **8**, 051003 (2015).

© Author(s) 2022

[38]N. Pant, Z. Deng, and E. Kioupakis, "High electron mobility of $Al_xGa_{1-x}N$ evaluated by unfolding the DFT band structure," Appl. Phys. Lett. **117**, 242105 (2020).
[39]N. Pant, W. Lee, N. Sanders, and E. Kioupakis, "Increasing the mobility and power-electronics figure of merit of AlGaN with atomically thin AlN/GaN digital-alloy superlattices," Appl. Phys. Lett. **121**, 032105 (2022).
[40]Y. Cho, C. S. Chang, K. Lee, M. Gong, K. Nomoto, M. Toita, L. J. Schowalter, D. A. Muller, D. Jena, and H. G. Xing, "Molecular beam homoepitaxy on bulk AlN enabled by aluminum-assisted surface cleaning," Appl. Phys. Lett. **116**, 172106 (2020).
[41]K. Lee, Y. Cho, L. J. Schowalter, M. Toita, H. G. Xing, and D. Jena, "Surface control and MBE growth diagram for homoepitaxy on single-crystal AlN substrates," Appl. Phys. Lett. **116**, 262102 (2020).
[42]J. Singhal, J. Encomendero, Y. Cho, L. van Deurzen, Z. Zhang, K. Nomoto, M. Toita, H. G. Xing, and D. Jena, "Molecular beam homoepitaxy of N-polar AlN on bulk AlN substrates," AIP Advances **12**, 095314 (2022).

© Author(s) 2022